Ultrasound in Med. & Biol. Vol. 17, No. 6, pp. 613–626, 1991
Printed in the U.S.A.

0301-5629/91 $3.00 + .00

●*Original Contribution*

IDENTIFYING ACOUSTIC SCATTERING SOURCES IN NORMAL RENAL PARENCHYMA FROM THE ANISOTROPY IN ACOUSTIC PROPERTIES

MICHAEL F. INSANA, TIMOTHY J. HALL and JAMES L. FISHBACK†
Department of Diagnostic Radiology and †Department of Pathology, University of Kansas Medical Center, Kansas City, Kansas 66103, USA

(*Received* 10 *October* 1990; *in final form* 6 *March* 1991)

Abstract—Acoustical and histological properties of dog kidney parenchyma are examined *in vitro* to determine sources of acoustic scattering in the normal kidney. The speed of sound, attenuation, backscatter, effective scatterer size and scattering strength were measured within the frequency range 1–15 MHz and at eight angles of incidence with respect to the predominant nephron orientation. Significant angular dependence, or anisotropy, was observed in backscatter coefficient and scattering strength estimates; attenuation was found to be weakly anisotropic. All three parameters, each measured at 19°C, exhibited values that were maximum for perpendicular incidence and minimum for parallel incidence. Speed of sound and scatterer size estimates were observed to be independent of scanning angle. Comparisons between these data for renal cortex and histological observations suggest that the glomerulus is the principal scatterer at low frequencies, and renal tubules and blood vessels at high frequencies.

Key Words: **Anisotropy, Attenuation, Backscatter, Correlation function, Kidney, Microscopic anatomy, Scatterer size, Scattering models, Scattering strength, Speed of sound, Tissue characterization, Ultrasound.**

1. INTRODUCTION

An ultimate goal of ultrasonic tissue characterization research is to discover the identity of tissue structures that scatter sound. Measurements of scattering cross sections (Bamber et al. 1981; O'Donnell et al. 1981) and acoustic microscopy data (Kessler et al. 1974) have indicated that connective tissues, fat, and water are the elements of acoustic scattering sources in soft tissues. However, identifying the exact histological structures has been difficult. In this paper, we study the anisotropic nature of acoustic properties for clues to identify the histological structures in renal parenchyma that backscatter ultrasound.

Acoustic anisotropy is the variation in acoustic properties with the angle of the incident sound field relative to the orientation of the medium interrogated. In biological tissues, acoustic anisotropy is associated with structural anisotropy, *i.e.*, the orientation of elastic substructures such as muscle fibers. For example, the backscatter and attenuation properties of tissues with oriented substructures, such as myocardium (Mottley and Miller 1988, 1990; Nicholas 1977), skeletal muscle (Nassiri 1979; Nicholas 1977), and kidney (Rubin et al. 1988;A Nicholas 1977), exhibit significant directional dependencies, while those in tissues with less-oriented substructures, such as liver, are considered isotropic (Mottley and Miller 1990; Campbell and Waag 1984). While these results underscore the importance of anisotropy in the interpretation of ultrasonography (Rubin et al. 1988), they also offer unique opportunities to identify scattering sources.

This paper details a series of *in vitro* experiments designed to measure the directional dependence of acoustic properties in normal renal parenchyma. Included are measurements of the speed of sound, attenuation coefficients, backscatter coefficients, scatterer size and scattering strength. Correlating these measurements with histological observations, we attempt to identify the anatomical structures in the kidney which dominate ultrasonic backscatter. As described below, the normal dog kidney is used because it is an excellent model for studying acoustic properties of the normal human kidney. The results are based on measurements from 11 kidneys obtained from nine dogs.

2. METHODS

2.1. *Renal anatomy and histology*

The gross anatomy of the dog kidney shows a radial symmetry of internal structure. A longitudinal

section through the center of a kidney may be divided both visually and sonographically into three annular regions. The cortex and medulla are the outer, relatively echolucent, parenchymal regions and the renal sinus is the central echogenic region. Macroscopically, renal parenchyma appear striated. Microscopic inspection reveals that these striae correspond to nephrons and blood vessels. The most uniform radial symmetry is found in the medulla, where numerous collecting ducts and Henle loops, *i.e.*, components of the nephron, radiate out from the center of the kidney (Fig. 1). Although these structures extend into the cortex, cortical symmetry is less uniform than in the medulla because of the addition of convoluted tubules and glomeruli, also components of the nephron. Each of the nephron's components have collagenous basement membranes, and therefore could present a sufficiently large acoustic impedance mismatch to scatter sound.

Spherically-shaped glomeruli, found only in the cortex, contain an inner capillary tuft surrounded by a collagenous Bowman's capsule. (Note: Our use of the term "glomerulus" indicates the combination of capillary tuft and Bowman's capsule. Although technically incorrect, this is the common usage of the term [Rouiller 1969].) Glomerular size and number vary significantly with the weight, surface area, and age of the animal. Kunkel (1930) estimated that there were 13 ± 4 glomeruli per mm^3 of adult dog kidney, with an average glomerular diameter of 173 ± 26 μm. Glomerular diameter was most closely related to body surface than any other feature, where the diameter was found to increase with surface area. The body weight of the 11 dogs studied by Kunkel ranged between 3.29–20.00 kg.

The external diameter of renal tubules varies with position along its length. In the dog, the average diameter of the proximal tubule is ~56 μm, the distal convoluted tubule is ~37 μm, and the thin segment of the loop of Henle is ~15 μm (Rouiller 1969; Sperber 1944). Basement membranes of the tubules are very thin and contain little collagen. Conversely, the intertubule spaces contain capillaries surrounded by basement membranes, interstitial tissue and a relatively high concentration of connective tissue elements (Rouiller 1969). The intertubule space occupies approximately 35% to 40% of the total kidney volume.

The dogs used in our experiments were random-source mongrels and larger than those reported by Kunkel: weights ranged between 20–25 kg. We studied tissue samples histologically from one of the dog kidneys used in our experiments to determine average diameters of glomeruli, renal tubules and blood ves-

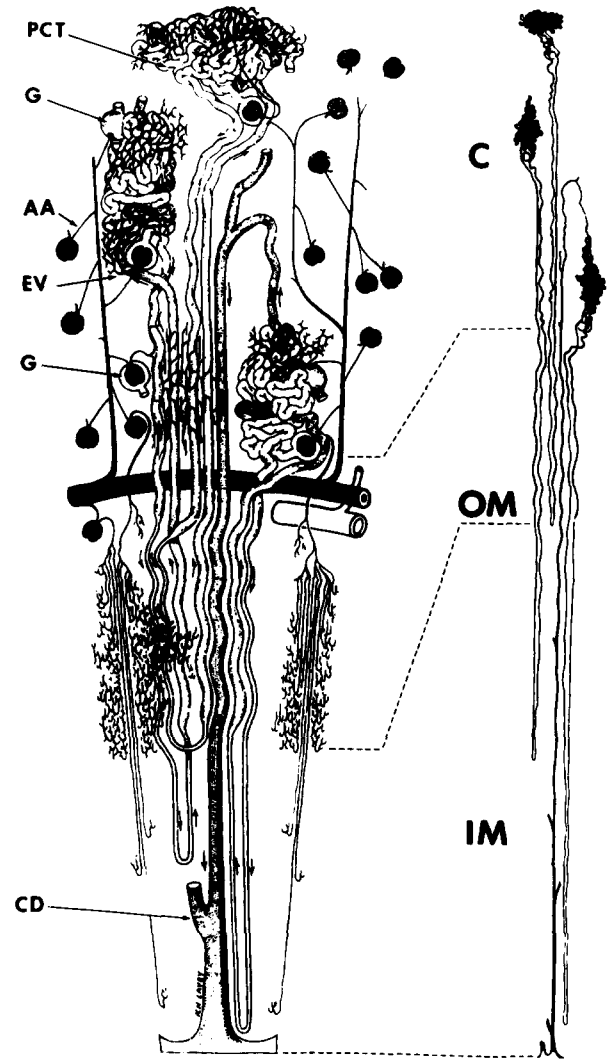

Fig. 1. The renal vascular organization of the dog is illustrated. The pattern in human kidneys is essentially identical. The vertical scale for three nephrons shown on the left is compressed. The same nephrons are shown undistorted on the right. AA, afferent arteriole; C, cortex; CD, collecting duct; EV, efferent vessels; G, glomerulus; IM, inner medulla; OM, outer medulla; PCT, proximal convoluted tubule. (Reproduced, with permission, from the *Annual Review of Physiology,* Vol. 42, © 1980 by Annual Reviews, Inc.)

sels. Cortical samples were fixed in 10% buffered formalin, embedded in paraffin, cut into thin sections, stained with hematoxylin-eosin and mounted on glass slides. Diameters were measured using a light microscope and a calibrated micrometer eyepiece. The resulting distributions, summarized in Fig. 2, show an average glomerular diameter of 216 ± 25 μm ($N = 39$) and an average cortical tubule diameter of 41 ± 8 μm ($N = 207$). Although no attempt was made to differentiate among the various tubule segments, only cortical samples were measured. Therefore mostly convoluted

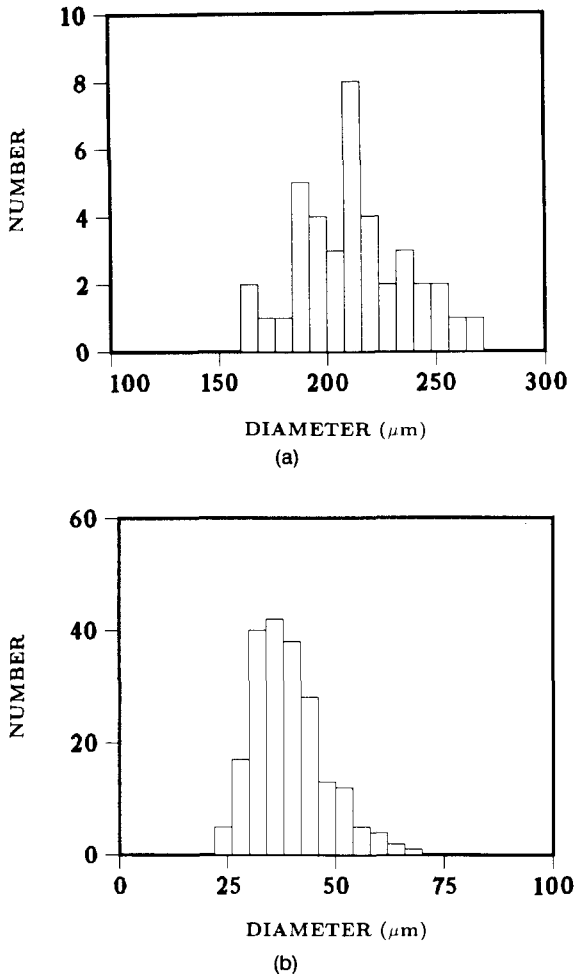

Fig. 2. Diameter distributions of nephron components in one dog kidney from light microscopy are shown. (a) The average glomerular diameter is 216 ± 25 μm. 39 glomeruli were sized. (b) The combined average renal tubule/blood vessel diameter is 41 ± 8 μm. 207 structures were sized. All measurements were increased by 7% to account for shrinkage.

tubule diameters were measured. All size estimates were corrected for an estimated 7% shrinkage due to sample preparation. Only those glomeruli in which the proximal tubule and afferent/efferent arteriole junction were evident were counted to ensure that measurements were made through the diameter of the glomerulus. Both cortical and juxtamedullary glomeruli were included. Glomerular diameters larger than those reported by Kunkel (1930) are consistent with the larger dog size. When sizing tubule and blood vessel diameters, we measured the short axis of only circular or nearly circular structures. Blood vessel and renal tubule measurements were then combined to produce a single distribution, since the average diameters were approximately equal. We found no reproducible method for measuring a characteristic dimension of the intertubule spaces.

The dog kidney is an excellent animal model for this study for several reasons. First, the acoustic properties of mammalian tissues are approximately the same for all species (Goss et al. 1978, 1979, 1980; Kessler 1973). Second, the microscopic anatomy of dog and human kidneys are essentially identical (Ganong 1981). Glomerular and tubule diameters are approximately the same in the adult human and large adult dog, but the human kidney is nearly twice as large with twice the number of nephrons (Clapp and Tisher 1989; Kunkel 1930). Third, the simple gross anatomy of the dog kidney has distinct advantages over the human kidney with respect to sample preparation. The dog kidney has a single renal crest and undivided medulla. In contrast, the human kidney has multiple papillae and the medulla is divided into a corresponding number of renal pyramids. Although the human renal cortex is undivided, as it is in the dog, it folds itself over each pyramid such that the nephron orientation is constantly changing—nephrons radiate out from the apex of each pyramid. Therefore it is very difficult to obtain a large piece of human cortex with a majority of the nephrons oriented in the same direction. Such samples are much easier to obtain with the dog kidney since the nephrons appear to radiate out from one point at the kidney center. Considering that the microscopic structures are the same, the dog kidney is a very good model for studying acoustic anisotropy in the human kidney.

2.2. *Sample preparation*

2.2.1. *Bulk acoustic measurements.* Fresh whole dog kidneys were studied within 24 hours postexcision. The organs were removed following unrelated experiments and stored in normal saline at 4°C overnight. The next morning, the renal capsule was removed and strips of cortex with parallel sides were cut as shown in Fig. 3. Dimensions of the cortical samples were approximately 10 mm from capsule to the cortical–medullary junction, 14 mm wide and 80 mm long. Tissue dimensions were measured before and after experimentation to detect swelling. Two strips from each kidney were selected, massaged to remove trapped air and cast in clear agar. The tissue-in-agar sample provided flat scanning surfaces and a well-defined nephron orientation. With these two samples, eight scanning directions could be obtained reproducibly. At the scanning angle $\varphi = 0°$, the beam axis was oriented parallel to the predominant nephron orientation and incident upon the capsule side of the cortex. At 180°, the beam axis was also parallel to the

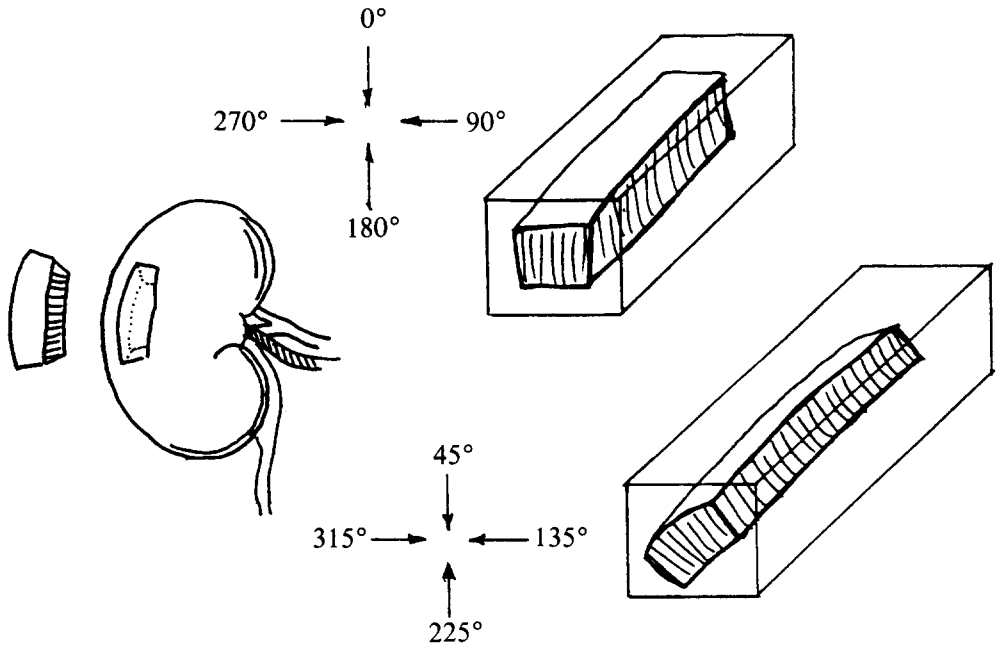

Fig. 3. Sample preparation is illustrated for bulk acoustic measurements from regions in the renal cortex. Scanning angles are indicated relative to the nephron orientation.

nephron, but incident upon the medullary side of the cortex. At 90° and 270°, the beam was perpendicular to the nephrons, *et cetera,* as indicated in Fig. 3.

The agar cast was prepared from a hot mixture of three grams of agar powder per 100 ml of fluid. The fluid was 7% n-propanol in normal saline. Alcohol was used to reduce the impedance mismatch between the tissue and agar. The agar mixture was maintained at 85°C until there were no visible air bubbles, cooled to 50°C and poured into a mold containing the tissue. Agar surrounded the tissue on all surfaces. Since the tissue is hypertonic relative to normal saline, experiments had to completed quickly (~2 h) to avoid significant tissue swelling. In this period of time, there was no evidence that the alcohol in the agar diffused into the tissue modifying the speed of sound. The agar casts were longer than the tissue samples, providing a region for measuring the sound speed and attenuation of the agar material itself.

2.2.2. *Acoustic macroscopy measurements.* A second type of sample preparation was needed to produce the speed of sound and attenuation images found in Fig. 7. Whole kidneys, cooled to 4°C, were cut into 5 mm thick slices along the short axis of the kidney with a meat slicer. The sliced tissue was then placed into a Lucite cylindrical ring, 5 mm in length and 50 mm in inside diameter. Molten agar was poured inside the ring, around the tissue and allowed to congeal. The cooled cylindrical ring sample with smooth and parallel surfaces was mounted on a fixture and placed in normal saline between a transmitter–receiver pair. There was little or no agar between the tissue and saline on the cylindrical surfaces.

2.3. *Measurement techniques*

2.3.1. *Attenuation and speed of sound.* Attenuation and speed of sound were measured in distilled and degassed water at 19°C and 35°C using a *narrow-band–through-transmission technique* similar to that described by Madsen et al. (1982). Sine-wave bursts of ultrasound were transmitted by 19 mm diameter transducers focused at 52 mm and received by a 0.6 mm diameter needle-type polymer hydrophone. The center of the sample was placed between a coaxial transmitter–receiver pair at the focus of the transmitter. The small diameter of the hydrophone minimized phase cancellation at the receiver (Marcus and Carstensen 1975; Goss et al. 1979). To minimize refraction artifacts (Turnbull et al. 1989), the hydrophone was placed as far from the tissue as possible. The amplitude transmitted at each frequency was kept sufficiently low to ensure that nonlinear propagation effects were negligible. Castor oil was used as a standard test media for verifying the accuracy of attenuation measurement techniques. Our attenuation measurements for castor oil agreed with those of Dunn et al. (1969) within 1% over the 1–12 MHz range.

Twenty-two measurements of the mid-burst amplitude and phase were read from an oscilloscope for each sample orientation and frequency. Twenty mea-

surements are of the tissue-in-agar cast, one measurement was made near the end of the sample through agar containing no tissue and one in distilled water without any agar or tissue inserted. The tissue-in-agar values used to compute sound speed and attenuation were an average of the twenty measurements.

The speed of sound in the agar, c_a, was calculated using the method described by Madsen et al. (1982). The speed of sound in the tissue, c_t, was then calculated relative to that of the agar using the equation

$$c_t(\varphi) = \frac{c_a}{1 + c_a\left(\frac{\Delta t}{d_t(\varphi)}\right)}, \quad (1)$$

where Δt is the shift in sine-wave phase with the tissue-in-agar sample in place relative to that of the agar-only sample, and $d_t(\varphi)$ is the tissue thickness at the scanning angle φ.

Attenuation coefficients for the agar, α_a, and the tissue-in-agar, α_{t+a}, samples were each calculated in dB/cm using the equation

$$\alpha(f,\varphi) = \frac{20}{d(\varphi)} \log_{10}\left(\frac{V_o(f,\varphi)}{V(f,\varphi)}\right), \quad (2)$$

where f is the frequency in MHz and V and V_o are the mid-burst voltage amplitudes with and without the sample inserted, respectively. The attenuation coefficient of the tissue, α_t, was determined from these values as follows:

$$\alpha_t(f,\varphi) = \frac{\alpha_{t+a}(f,\varphi)d_{t+a}(\varphi) - \alpha_a(f,\varphi)[d_{t+a}(\varphi) - d_t(\varphi)]}{d_t(\varphi)}, \quad (3)$$

where d_{t+a} is the total sample thickness. These techniques were used to determine average bulk properties as a function of frequency and orientation.

The spatial distribution of attenuation and sound speed within the kidney was determined using a low-frequency–through-transmission acoustic macroscope. This instrument is essentially the transmitter–receiver pair described above attached to a C-arm and moved in raster fashion within a plane perpendicular to the beam axis. A 0.5 mm raster scan increment was used. Thin tissue samples (see Section 2.2.2) were positioned in normal saline at the transmitter focus and oriented parallel to the scan plane. The narrow-band analysis described above was used to compute attenuation and sound speed images. However, to speed up data reduction, sine-wave bursts received by the hydrophone were digitally recorded at 100 Msamples per second, and data were reduced and displayed on a VAXstation 3500.

2.3.2. *Backscatter, scatterer size and scattering strength.* Backscatter coefficients, scatterer sizes and scattering strengths were measured in distilled water at 19°C using a *broad-band–pulse-echo technique.* Below is a brief summary of the analysis essential to these experiments. Derivation and experimental verification of the methods, including a description of the instrumentation, were described previously (Insana et al. 1990; Insana and Hall 1990).

Backscatter coefficients, σ_b, were estimated from the normalized power spectral density of echo signals using the equation

$$\sigma_b(f) = \frac{1.45\, R_1^2}{A_0 \Delta z} W(f), \quad (4)$$

where A_o is the area of the transducer aperture, Δz is the axial length of the range gated volume, R_1 is the on-axis distance between the transducer and the proximal surface of the gated volume and $W(f)$ is the average power spectral density of backscattered echo signals divided by that from a reference signal. The broad-band substitution method summarized by eqn. (4) requires the use of weakly-focused transducers, where the gated sample volume is placed near the radius of curvature. The surface of the planar reference reflector is also positioned at the radius of curvature, perpendicular to the beam axis.

Effective scatterer size and strength estimates are obtained by comparing theoretical models for σ_b to measured values as follows. First, we assume the tissue investigated can be modeled as randomly-positioned impedance fluctuations contained within an otherwise acoustically-uniform material. Statistical properties of random processes, such as echo signals from random media, are well characterized by correlation functions (Chernov 1960). Correlation functions statistically relate the acoustic properties of the medium at one location to those at surrounding locations and therefore characterize average properties of the scattering substructure, in particular the average scatterer size. For incoherent scattering from spherically-symmetric objects, the backscatter coefficient is modeled using the equation (Insana et al. 1990).

$$\sigma_b(f) = Cf^4 D^6 \bar{n}\gamma_0^2 F(f, D) \quad (5)$$

where C is a constant, f is frequency, D is the effective scatterer size, $\bar{n}\gamma_0^2$ is the effective scattering strength (*i.e.*, product of the average number of scatterers per unit volume and the mean-square variation in acoustic impedance per scatterer) and $F(f,D)$ is the acoustic

intensity form factor. The form factor is proportional to the Fourier transform of the correlation function for the medium, and therefore also describes average properties of the scattering substructure, but in this case in the frequency domain. With the previous assumptions, the form factor depends only on frequency and scatterer size (Insana et al. 1990). If the medium contains symmetric nonspherical scatterers and the axes of symmetry are aligned, the form factor will also be a function of scanning angle, $F(f,D,\varphi)$.

Second, the effective scatterer size estimate, D, is determined using least-squares analysis. A set of *modeled* form factors, $F(f)$, computed for different scatterer sizes are numerically fit to *measured* form factors, $\hat{F}(f)$, obtained from σ_b estimates for tissue. The model function that yields the smallest mean-squared error determines the size estimate; *e.g.*, Fig. 10, where each measured value, $\hat{F}(f)$, corresponding to one $\sigma_b(f)$ value, is compared to each modeled value, $F(f)$. Procedures for estimating scatterer sizes and scattering strengths have been described previously (Insana et al. 1990; Insana and Hall 1990).

Estimation accuracy is critically dependent upon knowing the appropriate correlation function for modeling form factors. The complexity of soft biological tissues makes it unlikely that accurate theoretical models will emerge. Investigators, therefore, have traditionally taken the empirical approach by choosing a few simple mathematical forms for the correlation function to model scattering from theory, *e.g.*, Gaussian and exponential functions, and comparing the results to measurements. Lizzi et al. (1987) found that both Gaussian and spherical correlation models explain backscatter data from the eye in terms of tissue morphology. Nicholas (1982) and Nassiri and Hill (1986) found that the exponential model was most appropriate for liver, although a multicomponent model was indicated. Bamber (1979) proposed the use of a three-component Gaussian model for the liver that was based on liver morphology. To the best of our knowledge, there have been no studies conducted to investigate correlation functions for the kidney. As we show in Section 3.3, backscatter data from kidney parenchyma clearly indicate a two-component Gaussian model.

3. RESULTS AND DISCUSSION

3.1. *Attenuation and speed of sound*

Average speeds of sound at 19°C for the cortex are plotted in Fig. 4 as a function of scanning angle. Since the speed of sound was independent of frequency and scanning angle, measurements corresponding to four frequencies between 1–12 MHz and eight scanning angles were averaged, and the result is 1540 ± 3 m/s. The same isotropic behavior in sound speed was observed at 35°C, although the average speed increased as summarized by Table 1. Our measurement of the speed of sound for dog kidney cortex at 35°C (1567 m/s) compares well to the measurements of Bowen et al. (1979) for dog kidney at 37°C (1569 m/s) and Turnbull et al. (1989) for human kidney at 37°C (1571 m/s). We also used the rate of change in speed per °C determined by Bowen et al. (1979) at 37°C (1.31 m/s/°C) to compare with our measurements at 19°C. The predicted value of 1543 m/s is very close to our measured value of 1540 m/s.

Average attenuations at 19°C and 5 MHz are plotted as a function of scanning angle in Fig. 5. Where the beam axis was perpendicular to the long axis of the nephron, attenuation was increased approximately 26% over nonperpendicular incidence. The anisotropy in attenuation was seen at other frequencies, as shown in Fig. 6. Measurements at 90° incidence were greater than those at 0° over the entire frequency range. Samples from four kidneys were used to obtain the data in Fig. 6, except at 5 MHz as noted in Fig. 5. Grouping measurements into those at perpendicular incidence (90°, 270°) and those at nonperpendicular incidence (0°, 45°, 135°, 180°, 225°, 315°) the functional form of the frequency dependence of attenuation was computed and summarized in Table 2.

Our average attenuation measurement at 5 MHz and nonperpendicular incidence are 2.32 ± 0.11 dB/cm at 19°C and 2.36 ± 0.11 dB/cm at 35°C. These values are very close to that at 5 MHz, 37°C reported recently by Turnbull et al. (1989) for human kidney

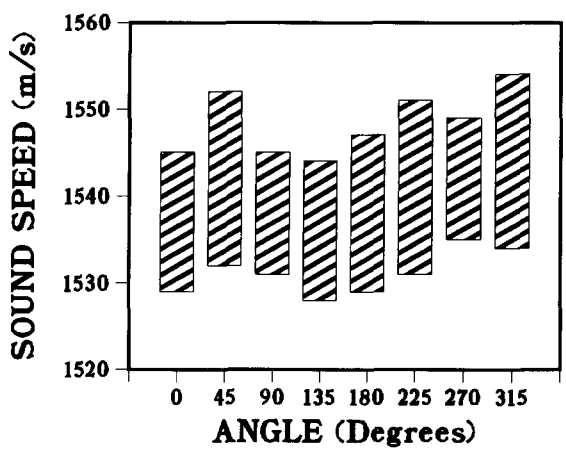

Fig. 4. The average speed of sound in the renal cortex is plotted as a function of scanning angle at 19°C. The bars indicate ± one standard deviation of the mean about the mean value, for an average of four frequencies and four dog kidney samples.

Table 1. Speed of sound in renal parenchyma.

Temperature	Cortex sound speed (m/s)	Medulla sound speed (m/s)
19°C	1540 ± 3	1512 ± 4
35°C	1567 ± 5	NA

(2.2 ± 0.6 dB/cm) and Le Croissette et al. (1979) for hog kidney (2 dB/cm). However, these measurements are approximately one half of those reported for dog kidney cortex by Kadaba et al. (1980) at 5.0 MHz (5.5 dB/cm), and for bovine kidney by Goldman and Hueter (1957) at 4.5 MHz (5 dB/cm) and Lele et al. (1976) at 5.0 MHz (5.2 dB/cm). Marcus and Carstensen (1975) and Goss et al. (1979) have shown that phase cancellation effects often produce attenuation values approximately twice those of methods in which these effects are minimized. Consequently, the lower range of values described above are probably closer to the intrinsic attenuation of kidney cortex. In summary, it is fair to assume that the attenuation in dog and human kidneys are comparable, particularly with respect to anisotropy. In addition, no significant dependence on tissue temperature was noted for the attenuation in the kidney at 5 MHz, which is consistent with the results of Kessler (1973) at much higher frequencies and Gammell et al. (1979) for the same frequency range.

Note that the anisotropy in attenuation for kidney does *not* follow the anisotropic patterns observed in skeletal (Nassiri et al. 1979) and cardiac (Mottley and Miller 1990) muscle. In both muscle studies cited, attenuation was greater for *parallel* incidence by a factor of ~2. Furthermore, Mottley and Miller (1990) found that the slope of the attenuation coefficient with frequency varied sinusoidally with scanning angle. For the kidney we find that the attenuation is slightly greater for *perpendicular* incidence and no obvious sinusoidal pattern is observed given the measurement uncertainties. Our results indicate that the mechanisms of attenuation in the kidney are very different from those in muscle. Since the angular dependence is fairly small and is correlated with the backscatter patterns (see Section 3.2), perhaps scattering is a larger fraction of attenuation in the kidney than it is in other tissues. However, it would be necessary to measure the total scattering cross section to make that determination.

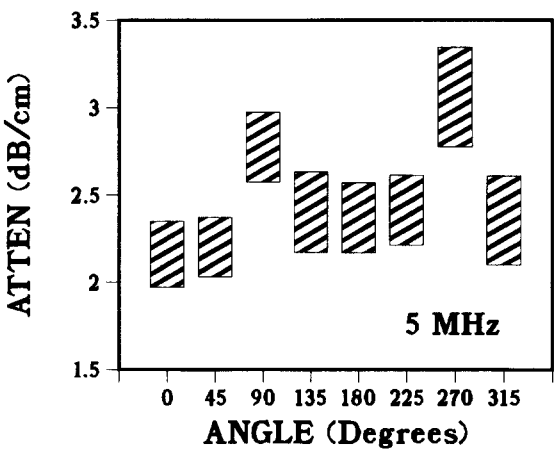

Fig. 5. The average attenuation coefficient in the renal cortex is plotted as a function of scanning angle at 5 MHz and 19°C. The results are averaged from measurements on eight kidneys from five dogs. The bars indicate ± one standard deviation of the mean about the mean value.

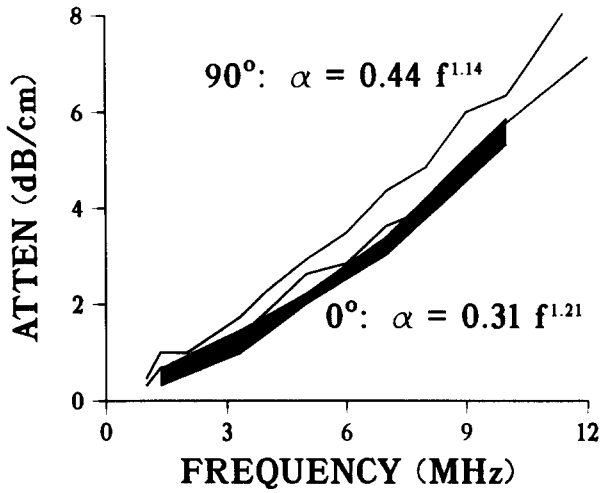

Fig. 6. Attenuation coefficients are plotted as a function of frequency for two scanning angles corresponding to perpendicular and parallel incidence. The dark region indicates the average attenuation for parallel incidence ± one standard deviation of the mean. The clear region between the two lines indicates the average attenuation for perpendicular incidence ± one standard deviation of the mean. Both data sets represent average measurements from four dog kidney samples, except at 5 MHz where eight kidney samples were used.

The acoustic macroscope was used to generate maps of attenuation and sound speed in the same low-frequency range as the bulk measurements to describe the spatial variation of these properties throughout

Table 2. Summary of attenuation measurements. $\alpha = \alpha_o f^n$, 1–12 MHz, 19°C.

Scanning angle	α_o (dB/cm/MHz^n)	n
90°, 270°	0.44	1.14
0°, 45°		
135°, 180°	0.40	1.08
225°, 315°		

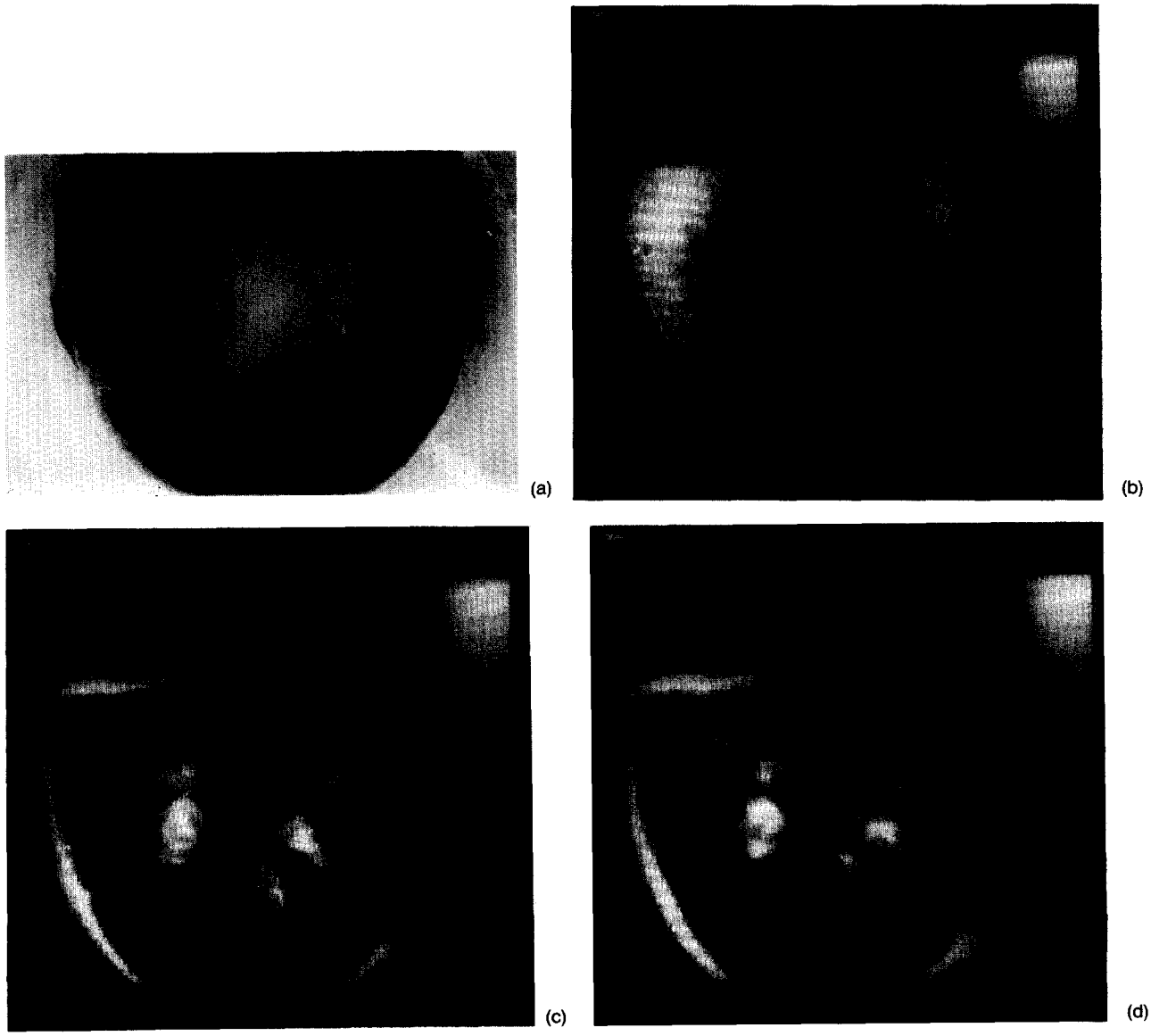

Fig. 7. (a) A photograph of a 5 mm-thick kidney slice used in forming acoustic macroscope images (b–d) is displayed. Speed of sound values range from 1485 m/s (darkest pixels) to 1565 m/s (brightest pixels). Details visible in the tissue (a) are also visible in the attenuation images (c) and (d), particularly at 10 MHz where striations in the cortex are clearly seen. Attenuation was estimated for the cortex (C), outer (OSOM), and inner (ISOM) stripes of the outer medulla, and inner medulla (IM) at 5 MHz (C = 2.8 ± 0.3 dB/cm, OSOM = 1.8 ± 0.2 dB/cm, ISOM = 2.3 ± 0.3 dB/cm, IM = 1.0 ± 0.2 dB/cm) and 10 MHz (C = 7.2 ± 0.9 dB/cm, OSOM = 3.8 ± 0.2 dB/cm, ISOM = 6.0 ± 0.8 dB/cm, IM = 2.6 ± 0.4 dB/cm).

the kidney. Images in Fig. 7 are of a 5 mm thick slice through a short axis plane obtained at 19°C. The beam axis is perpendicular to the alignment of the majority of nephrons. The sound speed image shows a gradual increase in c_t from the relatively dark, central medulla out to the brighter cortical periphery. The macroscope is well suited to measuring sound speed in the highly heterogeneous medulla. Examination of the central region in Fig. 7b shows that the sound speed in the medulla is significantly lower than that in the cortex at 19°C.

Unlike the speed of sound image, the attenuation images are highly detailed and reflect the same features seen by viewing the tissue directly. The apparently high attenuation seen at the boundaries, particularly at the kidney–agar boundary and arcuate arteries, is a refraction artifact as noted by Turnbull et al. (1989). The dark medullary region near the top is due to a section of renal calyx on the distal side of the sample. Kadaba et al. (1980) found no difference between bulk attenuation measurements of the cortex and medulla. Figures 7c and 7d, however, show signifi-

cant variations in attenuation among the cortex, inner and outer stripes of the outer medulla and inner medulla zones. These variations could be artifactual, since each zone has a different osmolality and therefore a different rate of swelling. A small amount of swelling was observed over the time of measurement, which could have produced the variations observed.

Accurate attenuation estimates are essential for determining backscatter properties of tissues.

3.2. *Backscatter and IBC*

Backscatter coefficients, measured in the cortex of one kidney at 19°C, are plotted in Fig. 8a as a function of frequency for four scanning angles. In general,

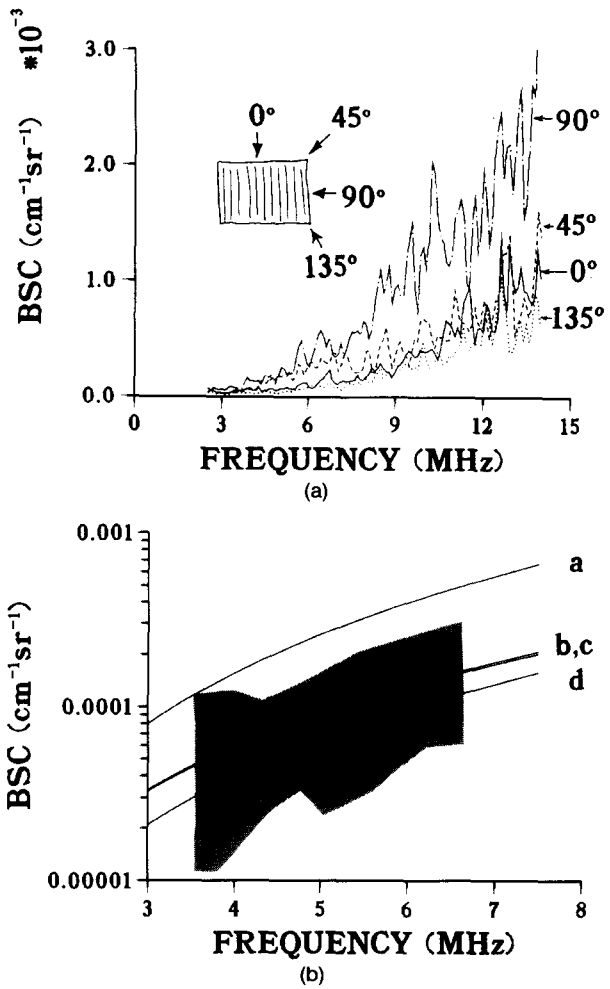

Fig. 8. Backscatter coefficients for kidney cortex (19°C) are plotted as a function of frequency. (a) Measurements for one sample at the four scanning angles indicated. (b) Data fit to a power law (Table 3) are plotted using a log scale. Curve **a** was determined by combining the data at 90° and 270°. Curve **b** corresponds to data at 45° and 225°, curve **c** corresponds to data at 135° and 315°, and curve **d** corresponds to data at 0° and 180°. The shaded region is adapted from the results for human kidney of Turnbull et al. (1989) for the purpose of comparison.

Table 3. Summary of backscatter measurements. $\sigma_b = \sigma_o f^m$, 2.5–14 MHz, 19°C.

Scanning angle	σ_o (cm^{-1} sr^{-1}) × 10^{-6}	m
0°, 180°	1.88	2.19
45°, 225°	3.68	1.98
90°, 270°	6.35	2.30
135°, 315°	3.71	1.99

measurements at angles modulo 180° are similar if the renal capsule is removed. There is a marked increase in σ_b for perpedicular incidence (90°, 270°) with respect to other angles—the same pattern seen with attenuation. These data are curve-fit to a power law (Table 3) and replotted in Fig. 8b on a semilog scale for comparison with data for human kidney at 37°C reported by Turnbull et al. (1989). In general, the two data sets agree except at perpendicular incidence. Turnbull et al. (1989) did not specify scanning angles.

To more clearly indicate trends in backscatter versus angle, σ_b values were summed over two frequency bands to compute the integrated backscatter coefficient (IBC). Selection of the frequency bands is discussed in Section 3.3. IBC versus scanning angle is plotted in Fig. 9. Plotted values are the average measurements from four kidneys at 19°C. At low frequencies (2.5–3.5 MHz) and particularly at high frequencies (7.0–15.0 MHz), there is a significant angular dependence. Mottley and Miller (1988) have shown that sinusoidal variations in backscatter with angle can occur in suspensions of aligned cylindrical scatterers. Applying this same conceptual model to scattering from renal parenchyma, we fit sine functions to the IBC data (Fig. 9) to estimate the amplitude and offset of the variations. The "best" two-parameter fit was determined by the sine wave with the minimum mean-square error. A period of 180° and a phase shift of 135° were assumed. The ratios of sine-wave maximum to minimum are 2.4 at low frequencies and 4.7 at high frequencies. Measurements at high frequencies fit the sine-wave model much more closely than did low-frequency measurements. Rubin et al. (1988) estimated a backscatter intensity max–min ratio of ~3 (*i.e.*, 4.7 dB) for sheep kidneys at 7.5 MHz. Considering the differences in frequency ranges, our measurements and those of Rubin et al. (1988) seem to agree.

3.3. *Scatterer size and strength*

As described in Section 2.3.2, the effective scatterer size is estimated as the result of fitting modeled form factors to those estimated from data. Examples of this procedure are shown in Fig. 10 for cortex at 19°C. A Gaussian correlation model was used

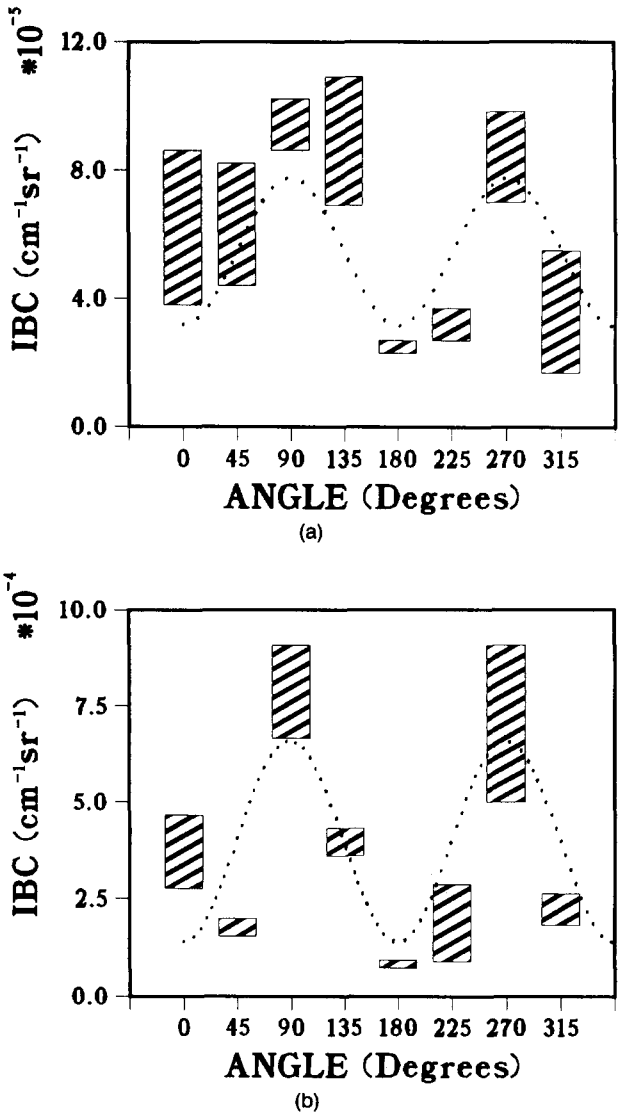

Fig. 9. Integrated backscatter coefficients (IBC) are shown as a function of scanning angle (19°C) at (a) low frequency (2.5–3.5 MHz) and (b) high frequency (7.0–15.0 MHz) bands. Bars indicate an average result from four kidneys ± one standard deviation of the mean. Dotted lines indicate a fit to a sinusoid.

throughout these studies, and the range of frequencies for the data presented corresponds to the 20 dB bandwidth of a 10 MHz transducer. Each of the four examples in Fig. 10 suggest at least two components to the measured form factor, $\hat{F}$. At 0° (parallel) incidence and for frequencies between 2.5–5.0 MHz, $\hat{F}$ is a sharply decreasing function indicating a relatively large scatterer size (Lizzi et al. 1987; Insana et al. 1990). Between 5.0–15.0 MHz, the decrease in $\hat{F}$ is less sharp indicating a smaller scatterer size. In this particular example, the best-fit model functions indicate an average scatterer size of 204 μm at low frequencies and 71 μm at high frequencies.

Increasing the scanning angle to 45° (Fig. 10), we can still identify two components with approximately the same scatterer sizes (174 μm and 73 μm). However, the zero-frequency intercept for the high-frequency component has increased relative to that at low frequencies. This trend continues at 90° (perpendicular) incidence, where the relative magnitude of the high-frequency component was largest. However, to measure the same two scatterer sizes seen at other angles, we had to narrow the low-frequency channel to 2.5–3.5 MHz and the high-frequency channel to 7.0–15.0 MHz. The behavior of the data between 3.5–7.0 MHz is interpreted as the sum of two scattering components with roughly equal contributions, neither dominating the backscatter signal. At frequencies below 3.5 MHz, large scatterers dominate the frequency dependence of backscatter, and at frequencies above 7.0 MHz, small scatterers dominate. Increasing the angle of incidence to 135°, the relative magnitude of the high-frequency component begins to decrease to the levels seen at 45°, and finally the data at 180° (not shown) looks similar to that at 0°. The cycle was seen to repeat over the next 180° of scanning angle. The two cycle pattern was clearly seen in all four of the kidneys examined.

We interpret the behavior of the form factor data as follows. The scatterer size estimates, as indicated by the frequency dependence of $\hat{F}$, are not changing significantly with φ. However, the scattering strength estimates, as indicated by the absolute magnitude of $\hat{F}$, oscillates with φ at a greater amplitude for high frequencies than low. Using the model defined by eqn (5), these trends support the theory that *changes in scattering strength, rather than size, are responsible for the anisotropy in backscatter from kidney parenchyma.*

Scatterer size estimates averaged using the data of four dog kidneys are plotted in Fig. 11. No obvious angle dependence is apparent from these data. Scatterer sizes averaged over all angles were 220 ± 15 μm at low frequencies (2.5–3.5 MHz for perpendicular incidence and 2.5–5.0 MHz otherwise) and 55 ± 10 μm at high frequencies (7.0–15.0 MHz for perpendicular incidence and 5.0–15.0 MHz otherwise).

The corresponding scattering strength measurements are plotted in Fig. 12. High-frequency estimates (Fig. 12b) exhibit a clear cyclic pattern similar to that for IBC measurements (Fig. 9b). At low frequencies (Fig. 12a), a cyclic pattern is present but less pronounced than that for IBC measurements in the same frequency range (Fig. 9a). Assuming the principal scatterer at low frequencies is the glomerulus (Section 3.4), these strength estimates are surprisingly low compared to measurements from blood. The scattering strength per scatterer, γ_0^2, can be estimated for kid-

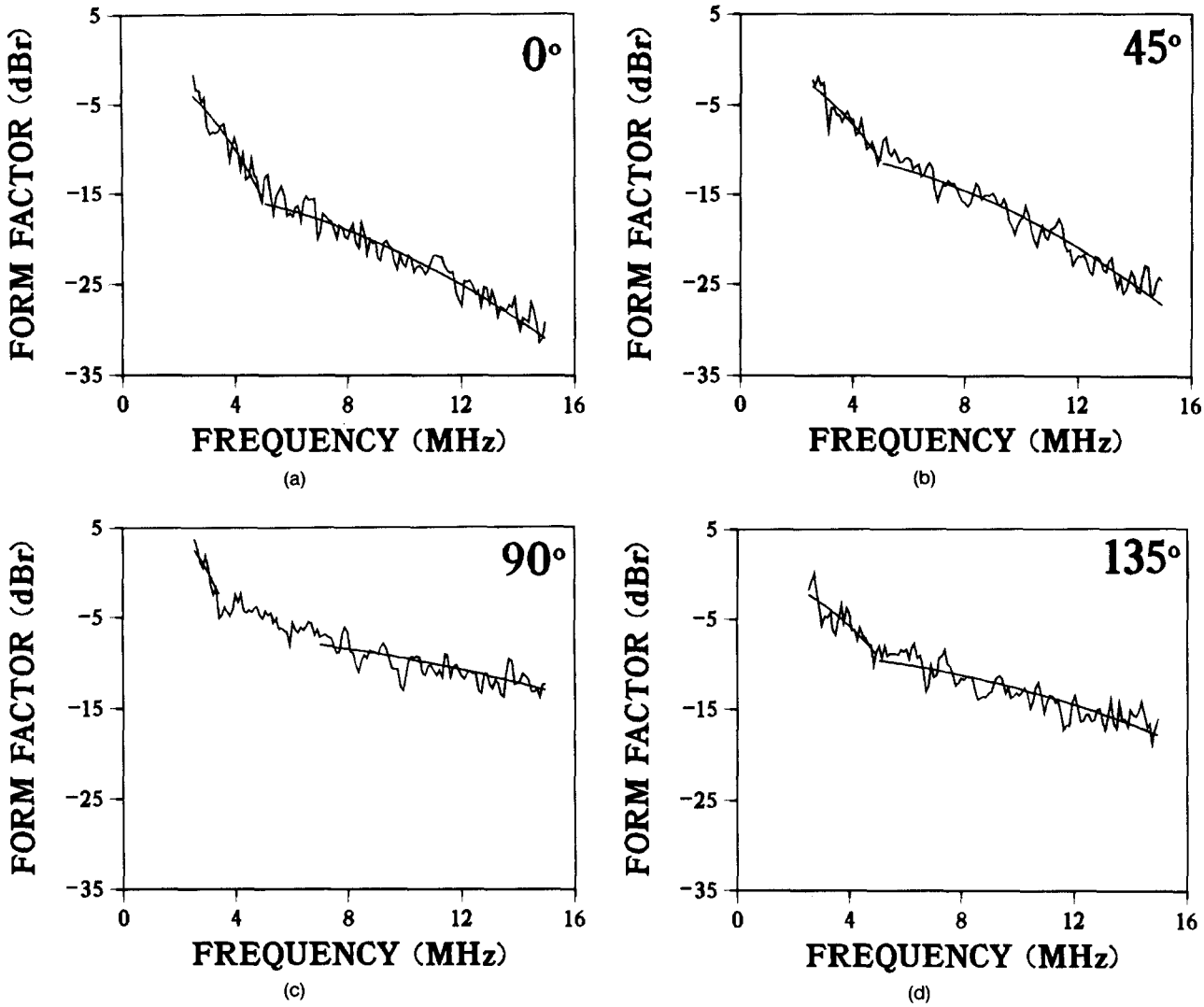

Fig. 10. Measured form factors (noisy lines) versus frequency are plotted for four scanning angles (a–d). Solid lines, denoting the best-fit model form factors, clearly indicate at least two scattering components—one at frequencies less than 5 MHz and one at frequencies greater than 5 MHz. The magnitude of the high frequency component relative to that at low frequencies is maximum for perpendicular incidence, 90°, and minimum for parallel incidence, 0°. See Section 3.3.

ney cortex from the ratio of the net strength, $\bar{n}\gamma_0^2$, and the average number density of scatterers, $\bar{n}$. Dividing the net strength estimate at low frequencies, ~0.01 mm^{-3}, by the average number density of glomeruli ~10 mm^{-3}, yields an average γ_0^2 value of ~0.001. From the density and compressibility of red blood cells and blood plasma (Urick 1947), γ_0^2 for blood is approximately 0.05. It is not likely that the scattering strength per red blood cell is 50 times that per glomerulus, unless collagen does not figure prominently in scattering from kidneys. More likely, the measurement uncertainties noted previously (Insana et al. 1990) are larger in tissue than in the test materials. It is also possible that kidney tissue structures are not fully described by this method as discussed below.

3.4. *Sources of scattering in normal renal cortex*

Combining the morphometric measurements from tissue histology with the acoustic measurements, we observed that the scatterer sizes corresponding to the two backscatter components have their counterparts in histologic observation. Hence, the following hypotheses regarding the sources of scattering in normal renal cortex are posed.

At low frequencies, *i.e.*, nominally below 5 MHz, scattering is dominated by glomeruli, more specifically Bowman's capsule. Our histologic measurement of glomerular diameter, 216 ± 25 μm, closely agrees with the acoustic measurement of 220 ± 15 μm. As expected, size estimates also are isotropic for randomly-positioned spherical scatterers. There is an an-

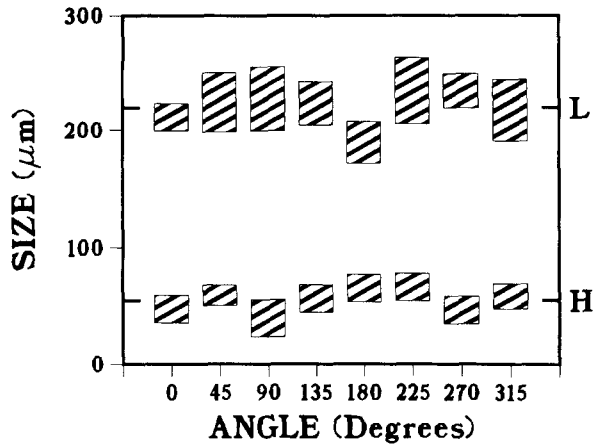

Fig. 11. Scatterer size estimates, D, are shown as a function of scanning angle (19°C). Bars indicate an average result from four kidneys ± one standard deviation of the mean. The average scatterer size at low frequencies (L) is 220 ± 15 μm, and the average scatterer size at high frequencies (H) is 55 ± 10 μm.

gle-dependent variability in the backscatter coefficient that is smaller in amplitude at low frequencies than high frequencies. This implies that, although glomeruli dominate the *frequency dependence of backscatter* at low frequencies, the contribution from aligned renal tubules and blood vessels to the *average backscatter intensity* at low frequencies is measurable. Note that the glomerulus is distended during normal physiologic activity and collapses after the circulation is interupted (Rouiller 1969), as it is in these *in vitro* results.

At high frequencies, *i.e.*, nominally above 5 MHz, scattering is dominated by renal tubules and blood vessels. The strongest evidence for this hypothesis is the angle dependence of backscatter. The cyclic variation in IBC observed is consistent with backscatter from a suspension of aligned cylindrical scatterers as demonstrated by Mottley and Miller (1988). Significant scattering from the connective tissue-filled intertubule space is unlikely, since there is no apparent axis of symmetry for this tissue component to cause the variation in IBC observed. Conclusions about the scatterer size estimates are less straightforward. In general, we observed an isotropic scatterer size with an average of 55 ± 10 μm, although a slight decrease in size may be seen for perpendicular incidence in Fig. 11 at high frequencies. It seems likely that scattering from convoluted tubules, *i.e.*, the numerous spatially-nonaligned segments of the nephron (Fig. 1), reduces the dependence of size on angle from that expected if only the aligned segments were present. Since the convoluted and aligned tubules have similar diameters, the size does not change with angle but the scattering strength does. The effective scatterer size at high frequencies (55 ± 10 μm) agrees reasonably well with our histological observations of tubules (41 ± 8 μm, Fig. 2) and those found in the literature (Rouiller 1969; Sperber 1944).

There is some doubt about the accuracy of this method for sizing kidney structures. Renal tubules are typically several millimeters long. If the tubule as a whole interacts with sound, as the variation in backscatter suggests, then the correlation length of the scatterer is not small compared to that of the range gate and transducer-beam directivity. That condition violates an important assumption intrinsic to the data reduction method (Insana et al. 1990). Supporting this idea is the fact that the minimum chi-square values obtained by fitting model functions to data are much larger at high frequencies than low frequencies. We must keep in mind, however, that large chi-square values could indicate a violation of the assumptions

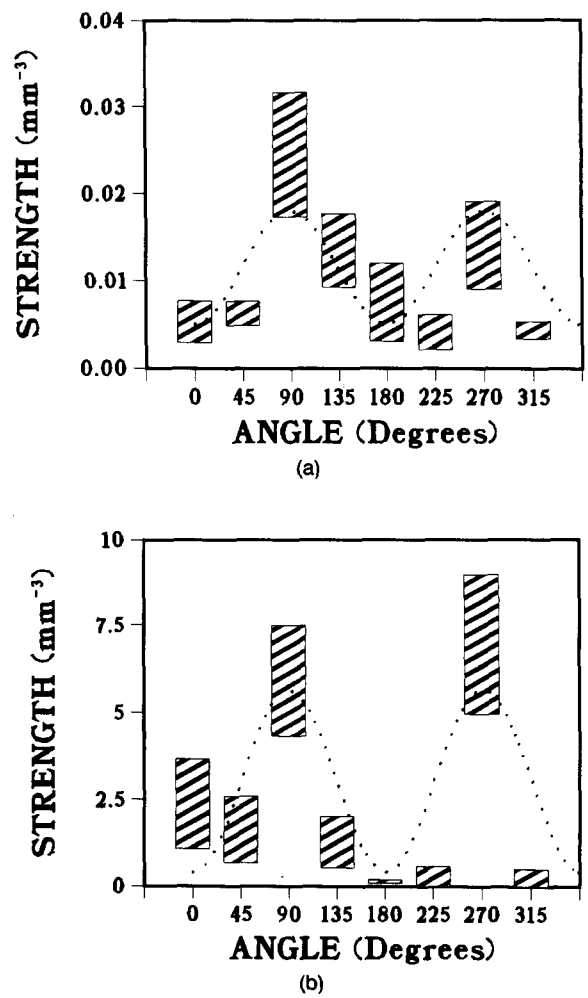

Fig. 12. Scattering strength estimates, $\bar{n}\gamma_0^2$, are shown as a function of scanning angle (19°C) for (a) low frequency and (b) high frequency. Bars indicate an average result from four kidneys ± one standard deviation of the mean. Dotted lines indicate a fit to a sinusoid.

or the need for a more sophisticated correlation model. Opposed to the idea that the method is invalid is the agreement between the acoustical and histological measurements. If only the thin collagenous basement membranes within the walls of the tubules interact with sound, then the oriented segments of tubules do not contribute significantly to the backscattered intensity at near-parallel incidence. In that case, the method's assumption holds and the results are physically descriptive. Resolving these issues rigorously is beyond the capabilities of the relatively simple scattering model currently employed in this analysis.

4. CONCLUSIONS

The anisotropy in acoustic backscatter observed in the renal cortex can be interpreted in terms of the tissue's microscopic anatomy. The data strongly indicate that glomeruli are the principal structures that backscatter sound at low ultrasonic frequencies. A weaker case may be made to suggest that renal tubules and blood vessels are the principal scatterers at high frequencies. The collagen in the basement membranes of these structures are likely candidates for scattering sources. Although based on measurements from dog kidneys, these results can be applied to the human kidney because of similarities in acoustic properties and microscopic anatomy.

Of the five examined, the most stable acoustic parameters for characterizing renal tissues are the speed of sound and scatterer size. Both estimates are independent of scanning angle, and the speed of sound is also independent of frequency. The agreement between the average glomerular diameter measured histologically and the effective scatterer size measurement is very good, typically within 10%. Several investigators have recently shown that glomerular size is an important diagnostic indicator of renal disease (Fogo et al. 1990; Reddi and Camerini-Davalos 1990). Consequently, the methods described in this paper could provide essential diagnostic information that may be obtained safely and inexpensively.

Acknowledgements—The authors gratefully acknowledge essential contributions by Glendon G. Cox, M.D., John Wood, Ph.D., Laurence Y. Cheung, M.D., and Ms. Rebecca J. Insana. This work was supported in part by grants from the Whitaker Foundation, West Trust, and NIH BRSG S07 RR05373.

Veterinary care was provided by the veterinary medical staff of the Animal Care Unit at the University of Kansas Medical Center. Animal use was approved by the Institutional Animal Care and Use Committee.

REFERENCES

Bamber, J. C. Theoretical modelling of the acoustic scattering structure of human liver. Acoust. Lett. 3:114–119; 1979.

Bamber, J. C.; Hill, C. R.; King, J. A. Acoustic properties of normal and cancerous human liver—II. Dependence on tissue structure. Ultrasound Med. Biol. 7:135–144; 1981.

Bowen, T.; Connor, W. G.; Nasoni, R. L.; Pifer, A. E.; Sholes, R. R. Measurement of temperature dependence of the velocity of ultrasound in soft tissues. In: Linzer, M., ed. Ultrasonic tissue characterization II, NBS Spec. Publ. 525. Washington, DC: U.S. Government Printing Office; 1979:57–61.

Campbell, J. A.; Waag, R. C. Measurements of calf liver ultrasonic differential and total scattering cross sections, J. Acoust. Soc. Am. 75:603–611; 1984.

Chernov, L. Wave propagation in a random medium. New York: McGraw-Hill; 1960: Chapter 1.

Clapp, W. L.; Tisher, C. C. Gross anatomy and development of the kidney. In: Tisher, C. C.; Brenner, B. M., eds. Renal pathology with clinical and functional correlation, Vol. 1. Philadelphia: J. B. Lippincott Co; 1989: chap. 2.

Dunn, F.; Edmonds, P. D.; Fry, W. J. Absorption and dispersion of ultrasound in biological media. In: Schwan, H. P., ed. Biological engineering. New York: McGraw-Hill; 1969:214.

Fogo, A.; Hawkins, E. P.; Berry, P. L.; Glick, A. D.; Chiang, M. L.; MacDonell, R. C.; Ichikawa, I. Glomerular hypertrophy in minimal change disease predicts subsequent progression to focal glomerular sclerosis. Kidney International. 38:116–123; 1990.

Gammell, P. M.; Le Croissette, D. H.; Heyser, R. C. Temperature and frequency dependence of ultrasonic attenuation in selected tissues. Ultrasound Med. Biol. 5:269–277; 1979.

Ganong, W. F. Review of Medical Physiology, 10th ed., Los Altos, CA: Lange Medical Publications; 1981: Chapter 38.

Goldman, D. E.; Hueter, T. F. Tabular data of the velocity and absorption of high-frequency sound in mammalian tissues. J. Acoust. Soc. Am. 28:35–37; 1956 and 29:655; 1957.

Goss, S. A.; Johnston, R. L.; Dunn, F. Compilation of empirical ultrasonic properties of mammalian tissues. J. Acoust. Soc. Am. 64:423–457; 1978.

Goss, S. A.; Frizzell, L. A.; Dunn, F. Ultrasonic absorption and attenuation on mammalian tissues. Ultrasound Med. Biol. 5:181–186; 1979.

Goss, S. A.; Johnston, R. L.; Dunn, F. Comprehensive compilation of empirical ultrasonic properties of mammalian tissues II. J. Acoust. Soc. Am. 68:93–108; 1980.

Insana, M. F.; Wagner, R. F.; Brown, D. G.; Hall, T. J. Describing small-scale structure in random media using pulse-echo ultrasound. J. Acoust. Soc. Am. 87:179–192; 1990.

Insana, M. F.; Hall, T. J. Parametric ultrasound imaging from backscatter coefficient measurements: Image formation and interpretation. Ultrasonic Imaging 12:245–267; 1990.

Kadaba, M. P.; Bhagat, P. K.; Wu, V. C. Attenuation and backscattering of ultrasound in freshly excised animal tissues. IEEE Trans. Biomed. Eng. BME-27:76–83; 1980.

Kessler, L. W. VHF ultrasonic attenuation in mammalian tissues. J. Acoust. Soc. Am. 53:1759–1760; 1973.

Kessler, L. W.; Fields, S. I.; Dunn, F. Acoustic microscopy of mammalian kidney. *J. Clin. Ultrasound* 2:317–320; 1974.

Kunkel, P. A. The number and size of the glomeruli in the kidney of several mammals. Bull. Johns Hopkins Hosp. 47:285–291; 1930.

Le Croissette, D. H.; Heyser, R. C.; Gammell, P. M.; Roseboro, J. A. The attenuation of selected soft tissues as a function of frequency. In: Linzer, M., ed. Ultrasonic tissue characterization II, NBS Spec. Publ. 525. Washington DC: U.S. Government Printing Office; 1979:101–108.

Lele, P. P.; Mansfield, A. B.; Murphy, A. I.; Namery, J.; Senapati, N. Tissue characterization by ultrasonic frequency-dependent attenuation and scattering. In: Linzer, M., ed. Ultrasonic tissue characterization, NBS Spec. Publ. 453. Washington, DC: U.S. Government Printing Office; 1976:167–196.

Lizzi, F. L.; Ostromogilsky, M.; Feleppa, E. J.; Rorke, M. C.; Yaremko, M. M. Relationship of ultrasonic spectral parameters to features of tissue microstructure. IEEE Trans. Ultrason. Ferroelec. Freq. Contr. UFFC-34:319–329; 1987.

Madsen, E. L.; Zagzebski, J. A.; Frank, G. R. Oil-in-gelatin dispersions for use as ultrasonically tissue-mimicking materials. Ultrasound Med. Biol. 8:277–287; 1982.

Marcus, P. W.; Carstensen, E. L. Problems with absorption mea-

surements of inhomogeneous solids. J. Acoust. Soc. Am. 58:1334–1335; 1975.
Mottley, J. G.; Miller, J. G. Anisotropy of the ultrasonic backscatter of myocardial tissue: I. Theory and measurement *in vitro*. J. Acoust. Soc. Am. 83:755–761; 1988.
Mottley, J. G.; Miller, J. G. Anisotropy of the ultrasonic attenuation in soft tissues: measurements *in vitro*. J. Acoust. Soc. Am. 88:1203–1210; 1990.
Nassiri, D. K.; Nicholas, D.; Hill, C. R. Attenuation of ultrasound in skeletal muscle. Ultrasonics 17:230–232; 1979.
Nassiri, D. K.; Hill, C. R. The use of angular acoustic scattering measurements to estimate structural parameters of human and animal tissues. J. Acoust. Soc. Am. 79:2048–2054; 1986.
Nicholas, D. Orientation and frequency dependence of backscattered energy and its clinical application. In: White, D. N., ed. Recent advances in ultrasound in biomedicine, Vol. 1. Forest Grove, OR: Research Studies Press; 1977:29–54.
Nicholas, D. Evaluation of backscattering coefficients for excised human tissues: Results, interpretation, and associated measurements. Ultrasound Med. Biol. 8:17–28; 1982.
O'Donnell, M.; Mimbs, J. W.; Miller, J. G. Relationship between collagen and ultrasonic backscatter in myocardial tissue. J. Acoust. Soc. Am. 69:580–588; 1981.
Reddi, A. S.; Camerini-Davalos, R. A. Diabetic nephropathy: An update. Arch. Intern. Med. 150:31–43; 1990.
Rouiller, C. General anatomy and histology of the kidney. In: Rouiller, C.; Muller, A. F., eds. The kidney: morphology, biochemistry, physiology, Vol. 1. New York: Academic Press; 1969: Chapter 2.
Rubin, J. M.; Carson, P. L.; Meyer, C. R. Anisotropic ultrasonic backscatter from the renal cortex. Ultrasound Med. Biol. 14:507–511; 1988.
Sperber, I. Studies on the mammalian kidney. Zool. Bidrag. Uppsala 22:249–431; 1944.
Turnbull, D. H.; Wilson, S. R.; Hine, A. L.; Foster, F. S. Ultrasonic characterization of selected renal tissues. Ultrasound Med. Biol. 15:241–253; 1989.
Urick, R. J. A sound velocity method for determining the compressibility of finely divided substances. J. Appl. Phys. 18:983–987; 1947.